Central Washington University

ScholarWorks@CWU

Fall 2007

Seismic Constraints on Slow Slip Events within the Cascadia Subduction Zone

Ana Cristina Aguiar
Central Washington University

Follow this and additional works at: https://digitalcommons.cwu.edu/etd

Part of the Geophysics and Seismology Commons, and the Tectonics and Structure Commons

Recommended Citation

SEISMIC CONSTRAINTS ON SLOW SLIP

EVENTS WITHIN THE CASCADIA

SUBDUCTION ZONE

A Thesis

Presented to

The Graduate Faculty

Central Washington University

In Partial Fulfillment

of the Requirements for the Degree

Master of Science

Geology

---

by

Ana Cristina Aguiar

October 2007

CENTRAL WASHINGTON UNIVERSITY

Graduate Studies

We hereby approve the thesis of

Ana Cristina Aguiar

Candidate for the degree of Master of Science

APPROVED FOR THE GRADUATE FACULTY

_____   _____
                                       Dr. Timothy Ian Melbourne, Committee Chair

_____   _____
                                       Dr. Charles Rubin

_____   _____
                                       Dr. Craig Scrivner

_____   _____
                                       Associate Vice President of Graduate Studies

ABSTRACT

SEISMIC CONSTRAINTS ON SLOW SLIP

EVENTS WITHIN THE CASCADIA

SUBDUCTION ZONE

by

Ana Cristina Aguiar

October 2007

Reanalysis of geodetic GPS time series from the Cascadia subduction zone have revealed at least 30 resolvable slow slip events along the megathrust, ranging from northern California to southern British Columbia, since 1997. Many of the smaller and more recent events are barely resolvable with GPS, but stand out clearly as tremor sequences. Since tremor bursts lasting less than 10-seconds are often visible across multiple stations, they offer the highest resolution for studying moment release through time. To test the hypothesis that tremor and transient deformation are two manifestations of the same faulting process, and to quantify the relative contribution of moment release during times of strain-transients versus other times, tremor bursts are systematically analyzed during the time period of June 2005 to February 2007. First, daily seismic files are consolidated from the Puget Basin of Washington State and SW British Columbia, where GPS density is highest. Seismic traces are included from the PNSN, the PBO borehole seismic network, and the EarthScope-funded CAFÉ experiment. Instrument

gain is removed, and then the data is decimated to 10 sps, rectified, its envelope is computed using a Hilbert transform, and lastly the envelopes are averaged from regionally adjacent stations to provide a single metric indicative of tremor activity. Then tremor duration is compared to equivalent moment slip inversions of corresponding GPS-derived deformation to obtain a model that relates hours of tremor to moment magnitude, showing that moment is directly proportional to the hours of tremor. Finally, to locate tremor during the January 2007 event, cross-correlated envelopes of band-pass filtered instruments are used. The location is determined by minimizing the L2-norm of the vector containing the differences between the measured and predicted stations offsets for a 3D grid of possible locations. Although the scatter is high, particularly in the depth, it is found here that tremor during the 2007 event propagates in a northwesterly direction beneath the eastern Olympics Range over a 3-week period.

ACKNOWLEDGMENTS

TABLE OF CONTENTS

LIST OF TABLES

LIST OF FIGURES

CHAPTER I

INTRODUCTION

The Cascadia subduction zone of the northwestern United States and
southwestern Canada is a ~1000-km thrust fault that stretches from northern California to
Vancouver Island. Here, the Juan de Fuca plate is subducted beneath the North America
plate. This interface is thought to be seismically active, in that magnitude $M_w \sim 9$ thrust
earthquakes have ruptured the shallow interface repeatedly every several hundred years
(Atwater *et al.*, 1987; Satake *et al.*, 1996; Atwater *et al.*, 1997). There is geological and
historical evidence that suggests that the last one of these large events occurred in 1700
as a M_w 9 earthquake (Satake *et al.*, 1996; Satake *et al.*, 2003; Atwater *et al.*, 2005).
About 5 years ago it was determined that another process occurs in this subduction zone
and in other subduction zones of the world.

It has been recognized that a large portion of the deeper Cascadia subduction zone
is aseismically slipping, down-dip of the locked zone, at around 25 km to 45 km depth
(Figure 1). Evidence for this was provided by continuous geodetic measurements from
seven global positioning system (GPS) sites that measured a transient reversal from the
long term northeastward motion into an extension SE-directed motion. (Dragert *et al.*,
2001). This process was also observed with GPS in other places of the world after a few
large subduction earthquakes. During the weeks after these events; such as the 1995 $M_w =$
8.0 Jalisco (Mexico) event, the 1994 $M_w = 7.7$ Sanriku (Japan) event, and the 2001 $M_w =$
8.4 Peru event, there was postseismic motion with additional moment release (Melbourne
et al., 2002).

1
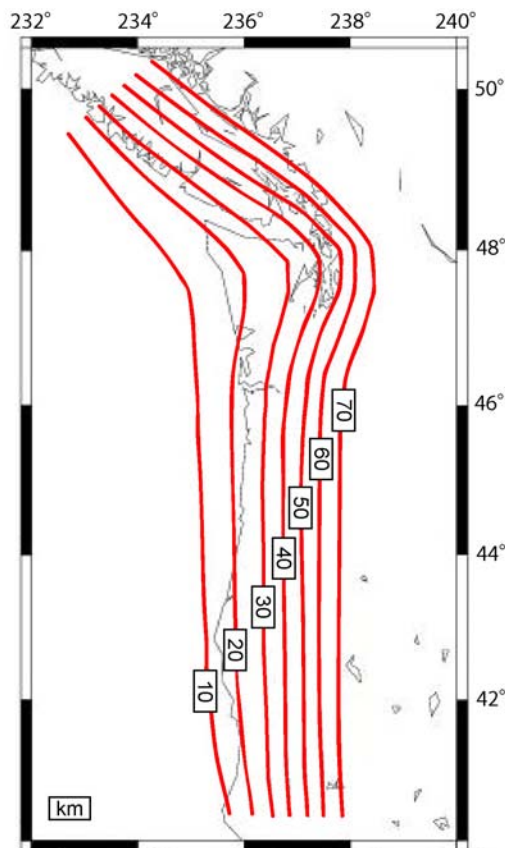
Figure 1. Depth contours of the Cascadia subduction zone. The subduction zone starts in northern California and ends at Vancouver Island. The black numbers represent the depth on each of the contours (red).

It was first thought that this type of event released large amounts of strain energy without any detectable seismic shaking (Linde *et al.*, 1988), but it was later recognized that a subtle seismic signature does accompany this slow creep. The slip events were assumed to have rupture rates lower than those that can be detected by most forms of seismic instrumentation (Melbourne *et al.*, 2002) and it was not possible to see this signal before. As mentioned before, slow slip events (SSE) like these have now been found in many convergent margins other than Cascadia such as Mexico, Alaska, Japan and Costa Rica, lasting from a few days to as long as a few years (Ozawa *et al.*, 2002).

In the case of Cascadia, initial studies showed that these events have been taking place every 14.5 ± 1 months for the past 10 years (Miller *et al.*, 2002). More recent studies demonstrate that the periodicity varies within the different areas that form the Cascadia subduction zone: there is a periodicity of 10.9 ± 1.2 months under northern California and an 18 ± 2 month periodicity offshore central Oregon (Szeliga *et al.*, 2004). This regular and cyclical nature of the transient events indicates that they are a fundamental mode of strain release in subduction zones, and they may contribute to the strain build-up that can result in a great earthquake.

The first seismic signals related to the slow slip events were originally noticed in the Japan fore arc region, where the Philippine Sea plate is subducting under the Eurasian plate. Using a borehole seismograph network, Japanese scientists were able to find tremor bursts that lasted a few minutes to a few days (Obara, 2002). Afterward, in Cascadia these non-volcanic tremors were recognized using the regional surface seismic network. These are pulsating, deep tremor-like seismic signals (Rogers and Dragert, 2003) that are usually observed at active volcanic areas. Besides Japan and Cascadia, this type of nonvolcanic tremor has also been detected in the San Andreas fault (Nadeau and Dolec, 2005) and the Alaskan subduction zone (Peterson *et al.*, 2005).

Tremor location is difficult, primarily because they do not look like regular earthquake waves in a seismogram, with discernible P and S phases. Instead, tremor is very clustered, emergent and noisy, and the onset time is extremely hard to pick, obfuscating depth constraints. Also, they have a high frequency content of 1 to 5 Hz (lower than regular earthquakes) which causes them to be sensitive to small-scale crustal

structures, therefore making them even noisier signals by the time they reach the surface seismometers.

The first approach to analyzing the nonvolcanic episodic tremor-and-slip (ETS) in Cascadia assumed that tremor bursts were located near or along the subduction interface (Rogers and Dragert, 2003). But by using a source-scanning algorithm (Kao *et al.*, 2005), which uses a brightness function on the grid points of the subduction zone to identify the existence of seismic sources in time and space, it was determined that tremor bursts are widely distributed over a 40-km depth range, and that they are bounded approximately by the surface projections of 30- and 45-km depth contours of the subduction plate interface (Kao *et al.*, 2005). When the seismic data are Band-pass filtered to 1–6 Hz and rectified, signals of the tremor prove to be strongest on the horizontal components. Using a one dimensional S-wave velocity model, hypocenters of tremor bursts were determined with depth errors of 5 to 10 km. The results of this method were consistent with the last result, which were that tremors signals have an apparent velocity of 3.8–4.2 km/s and that tremor depths are distributed over a wide range (including the overriding crust and the subducting slab) greater than the errors (McCausland *et al.*, 2005). The observed depth range implied that tremors could be associated with the variation of stress field induced by the transient slip events.

These tremor bursts have not been located directly on the plate interface, but there is little doubt that they are related to the slow slip events. So it was necessary to explain their existence with another process related to the slip. The process that has been suggested is the movement of fluids: dehydration of fluids on the plate interface to its

surroundings traveling through cracks might cause these tremor bursts by changing the pressure in the system (Obara, 2002; Kao *et al.*, 2005; McCausland *et al.*, 2005).

In 2006 it was discovered in the Nankai subduction zone that there are also other mechanisms releasing stress in the transition zone during these GPS-detectable events. These new signals where named low frequency earthquakes (LFE) because it is usually only possible to identify their S-wave arrivals (Shelly *et al.*, 2006). These events were located to the plate interface and have a shear slip mechanism. Cross-correlating LFE suggested that low frequency tremor may be a superposition of these LFE (Shelly *et al.*, 2006); in other words, that tremor bursts also originate from small thrust faults along the plate interface.

After the LFE were found, another signal was identified between the tremor bursts in Japan. These where named very low frequency (VLF) earthquakes. They have a very long period of as much as 20 s and are indeed happening at the same time and also have a similar migration as the tremor bursts (Ito *et al.*, 2006). The VLF earthquakes have a thrust mechanism and are bound to the plate interface at depths of 30–35 km (Ito *et al.*, 2006). This result is important because it brings us one step closer to understanding the mechanism triggering slow slip events.

To further investigate the mechanism of the LFE, Ide *et al.* (2007) analyzed the first arrival P-wave and an inversion of the empirical moment tensor of the S-wave separately. Both analyses yield the same result; that is, that LFE are a result of shear slip on a low angle fault (Ide *et al.*, 2007), and they are consistent with the SSE thrust mechanisms shown in previous studies (Hirose and Obara, 2005). Finally, by using a

match filter technique on the tremor bursts to see if they correlate with the LFE, it was found that during high tremor times the LFE sequences are almost continuous; so tremor signals are now believed to be a swarm of LFE generated by many small shear slip events on the plate interface (Shelly *et al.*, 2007).

Cascadia is one of the largest subduction zones on Earth, akin to the Sunda megathrust which produced the 2004 Sumatra (M_w 9.3, 300 000 deaths) great earthquake, and populated with 6–7 million people on the forearc. With the discovery of the SSE and ETS with GPS, we now have a major new constraint on the Cascadia energy budget. GPS is limited by daily measurements, sparse coverage, and non-unique inversions. Tremor by contrast, clearly gives moment-by-moment details of slip evolution so it can be used as a higher resolution instrument to find out more about these SSE.

If this model is correct, and given the noted difficulty in determining hypocentral locations (particularly depth for tremor sources), it makes sense to ascertain whether tremor follows magnitude—frequency relationships inferred for other tectonic regimes. Since magnitudes cannot be assigned to tremor bursts until the source of the mechanism is better understood, it makes sense to instead attempt to quantify the frequency— duration aspects of tremor, whether it varies over time, and in particular whether it varies during the largest, GPS-detectable slow slip events.

The importance of doing further investigation on this topic is that there are reasons to think that big megathrust events will be triggered by SSE, which, as mentioned before, are not only recognized in Cascadia but also in other faults such as the San Andreas fault (Nadeau and Dolec, 2005), and are likely ubiquitous in all active faults.

Furthermore, these SSE are dissipating energy at the lower end of the locked zone, so they delineate the seismic hazard to cities, such as Seattle, that lie near the top of the forearc of large subduction zones. Finally, to asses this seismic hazard it is also necessary to know by what amount they are reducing the strain that might be released by the large subduction zone earthquakes.

The specific aspects of tremor addressed here are as follows:

1. Does tremor follow anything resembling known frequency—magnitude relationships? Is it a log–linear relationship and what are the b-values?

2. If not, then what does a typical distribution look like?

3. Does the frequency—duration relationship change during the largest slow earthquakes?

4. What percentage of total tremor time is released during an SSE versus all the other time?

5. Does average tremor amplitude increase during GPS events, or is it only the duration that varies during this time?

6. Where are tremor sources located during the January 2007 event?

7. Does tremor coincide with the down dip limit of transient slip as inferred from GPS inversions?

These questions were addressed under the assumption that GPS-observed deformation transients and tremor bursts are different manifestations of the same shear dislocation process at depth.

CHAPTER II

DATA PROCESSING

There are various seismic networks across the Pacific Northwest: the Pacific

Northwest Seismographic Network (PNSN), a surface network run by the United States

Geological Survey and the University of Washington that monitors seismicity in the

states of Washington and Oregon; the Plate Boundary Observatory (PBO) borehole

network, which is part of the EarthScope project run by UNAVCO, Inc.; the

Transportable Array (TA), which is part of the Incorporated Research Institutions for

Seismology (IRIS) and EarthScope USArray; and the EarthScope funded Cascadia

Arrays For EarthScope (CAFE) experiment network. Seismic data from these four

different networks were obtained from the IRIS Data Management Center (DMC) Web

site covering the time span from July of 2005 to February of 2007 (Figure 2). This time

period was selected mainly because it contains two of the latest GPS-detectable events

which are the September 2005 event and the January 2007 event.

The data, after they had been requested, were delivered via file transfer protocol

(ftp) in SEED format. The seed files were converted to a format suitable for use in the

Seismic Analysis Code (SAC) program. This program is a tool used to make detailed

analysis of any kind of seismic data.

Merging the Data

The data, as stored by IRIS comes in many separate pieces, including parts of a

day or even parts of two different days together. The first step was to merge all the
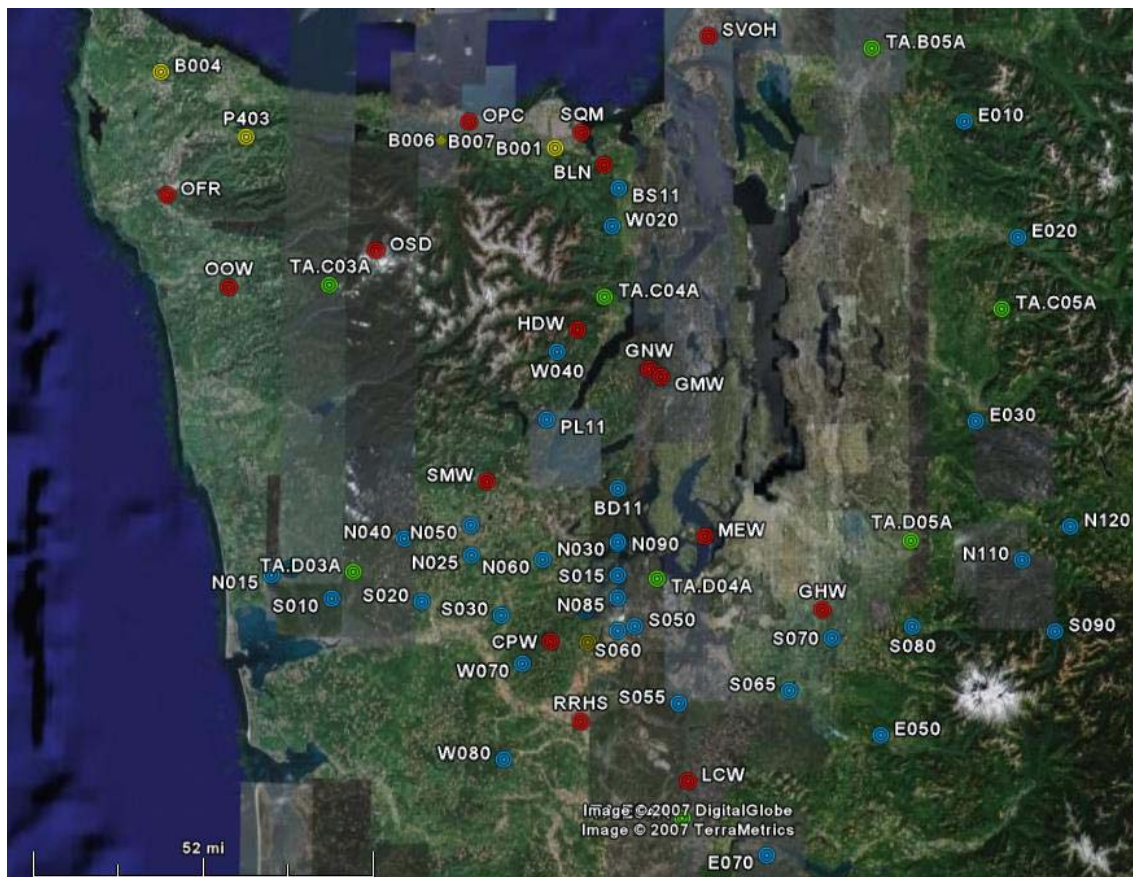
Figure 2. Map of stations from the four seismic networks used. The different colors represent the different networks. Red represents the Pacific Northwest Seismographic Network stations, yellow represents the Plate Boundary Observatory stations, green represents the Transportable Array stations and blue represents the Cascadia Array For EarthScope stations. Modified from Google Earth.

pieces of data into daily files so the data could be analyzed one day at a time and different

stations could be compared using a single metric. To do this it was necessary to first cut

files with parts of two different days in them, and this was accomplished using the

program called chop_day.pl. This program would take each sac file, open it using SAC,

cut the parts of different days and rename the new cut files using the respective date and

time. After running chop_day.pl on all the files, the seismic data were ready to be

merged. A new program was written for this, dailify.pl, and it uses SAC to read all the

sac files for one day and merge them together into one file containing a complete day of

data (Figure 3). The files created by this program where named with the format

YYYY.DOY.STA.COMP.sac; as an example the file 2006.204.CPW.EHZ.sac would be

the file corresponding to the year 2006, day of year 204, station CPW, and component

EHZ.
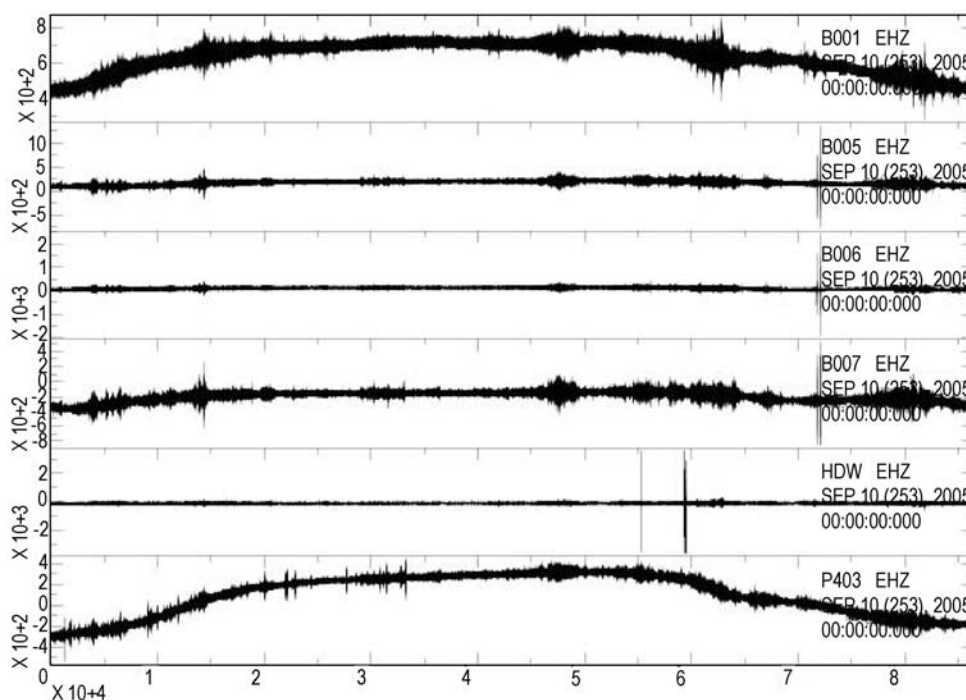
Figure 3. Example of merged data. The merging process was done for six different stations on September 10 of 2005. This data shows various tremor bursts across the day. This is for day 253 of 2005.

Data Reduction

Every daily file is around 30 Mb in size, so to be able to work with years of data

in a time efficient way, it is necessary to bring this number down. Before the size can be

reduced, the first step is to remove the velocity sensitivity or gain of each station. Station

gains vary as a consequence of the different types of stations: broadband, short-period,

etc. By doing this, all the stations can be compared on the same scale, which is required

to obtain the averages of the seismic files for one day. To do this, the program degain.pl

reads in a seismic file containing one day of data and gets the gain information for each

station and each component from a text file containing the velocity sensitivity in counts

per meter per second. Using a SAC module, the gain is removed from each of the daily

files dividing each data point by the gain corresponding to that station and component.

Then it outputs a new file containing the degained data.

Now, to finally reduce the size of the daily files, it is necessary to decimate the

data. The raw data contains files that are 100 samples per second (sps), and by using the

program decimate.pl (created for this same purpose), which also uses a SAC module, the

seismic files are decimated to 10 sps each. These new files are around 3.2 to 3.4 Mb each,

which is significantly smaller than the raw data (~ 30 Mb).

Data Selection

Now that the size of the seismic files has been reduced, a data selection has to be

done. In order to average the files, it is necessary that all files that are to be merged for a

particular day have the same number of points. The files that contain data for less than 23

hours of one day are discarded, and the remaining files are cut to the number of points of

the smallest file remaining (longer than 23 hours) for that same day of the year. This

selection and cutting processes are done using the Perl program called cut.pl that uses a

SAC module to do all this. The remaining files that have been cut have to go through

another selection. It is necessary to make sure that these files all start at 00:00:00 hours of

the day. If they don't, they are dropped because by the time the files are averaged, they

would be shifted to the right giving a wrong average. This final selection process is done with final_cut.pl also using a SAC module.

Calculating the Averages

The averages of each day of the seismic data are done using the envelope function of the files. After selecting the data to be used in the analysis, the envelopes of the files can be calculated. These are essential for automatically quantifying tremor burst, because they give a positive scale of the seismic trace. The Perl program envelope.pl was created for this purpose. This program opens the file in SAC, squares it, applies the square root, and then calculates the envelope function using a Hilbert transform. This program outputs a new file for each seismic file containing its envelope function (Figure 4a).

The averages are calculated for each day of the year. Using the program average.pl, the files for one day of the year and different regionally adjacent stations are summed up and then divided by the number of files summed to get the average of that day (Figure 4b).

Summary

Here I present a summary of Perl codes written to process the data in the order they had to be run, their names, and their purpose (Table 1). This may serve as a tool for further use of the programs outside of this thesis.
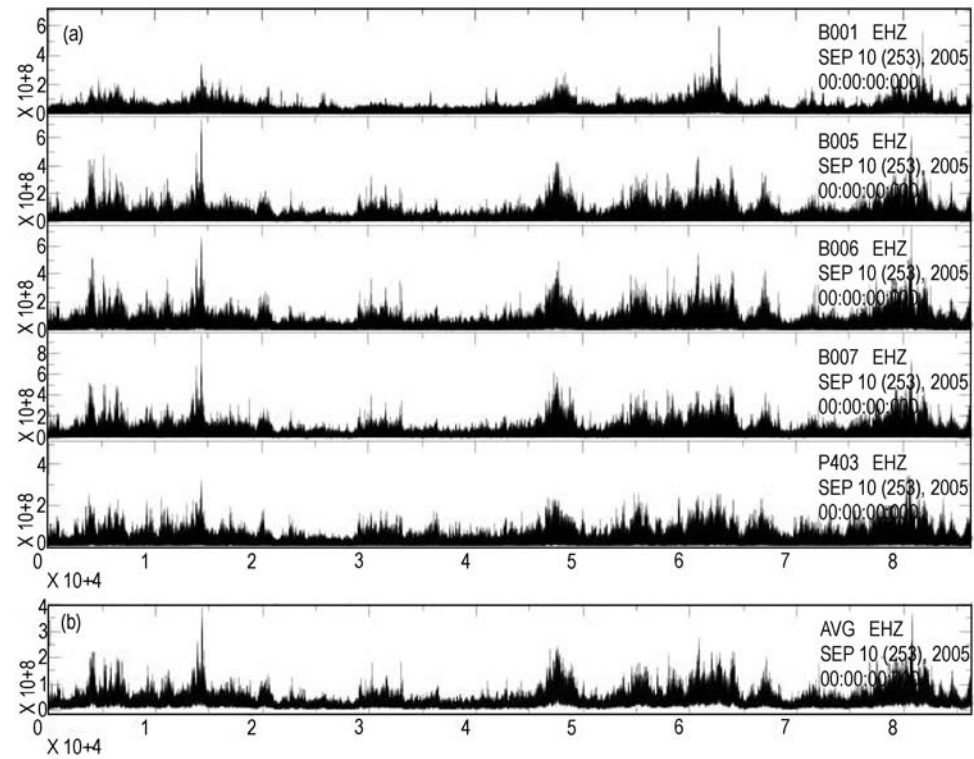
Figure 4. Example of envelope functions. (a) Envelope functions of the seismic data from 5 different stations that survived the data processing for day 253 of 2005. Each of the spikes across the data represents a tremor burst that might be composed of more bursts. (b) Average of those same five envelope functions.

Table 1
Summary of Programs Written for Data Processing

Program Name	Function
chop_day.pl	Separates files that contain data for different days of the year and creates new files with the separated pieces of data.
dailify.pl	Gets the chopped files (output of chop_day.pl) and merges them into daily files.
degain.pl	Removes the gain of all the different stations of which the seismic data come from.
decimate.pl	Turns the degained files (output of degain.pl), which are 100 sps files, into 10 sps files
cut.pl	Eliminates daily files shorter than 23 hours, and then cuts the remaining files to the number of points of the shortest file in the list, so they all have the same number of points.
final_cut.pl	From the remaining files (output of cut.pl), it eliminates the ones that do not start at the beginning of the day (time 00:00:00).
envelope.pl	Uses the output of final_cut.pl and calculates the envelope function of them.
average.pl	Takes all the envelope files (output of envelope.pl) and calculates an average of these files for each day of the year separately.

CHAPTER III

TREMOR QUANTIFICATION

Once the regional averages are computed, it is assumed that any signal that survives the envelope stacks is tectonic in origin, given that local ground noise should not stack coherently. For each regional averaged file, tremor is identified and summed in the following manner: all times in which the regional envelope average exceeds a threshold value of the velocity amplitude is considered to be active tremor; less than this value is considered noise. Picking the threshold is a difficult task and it is done manually, typically using a day where tremor bursts are obvious (Figure 5).
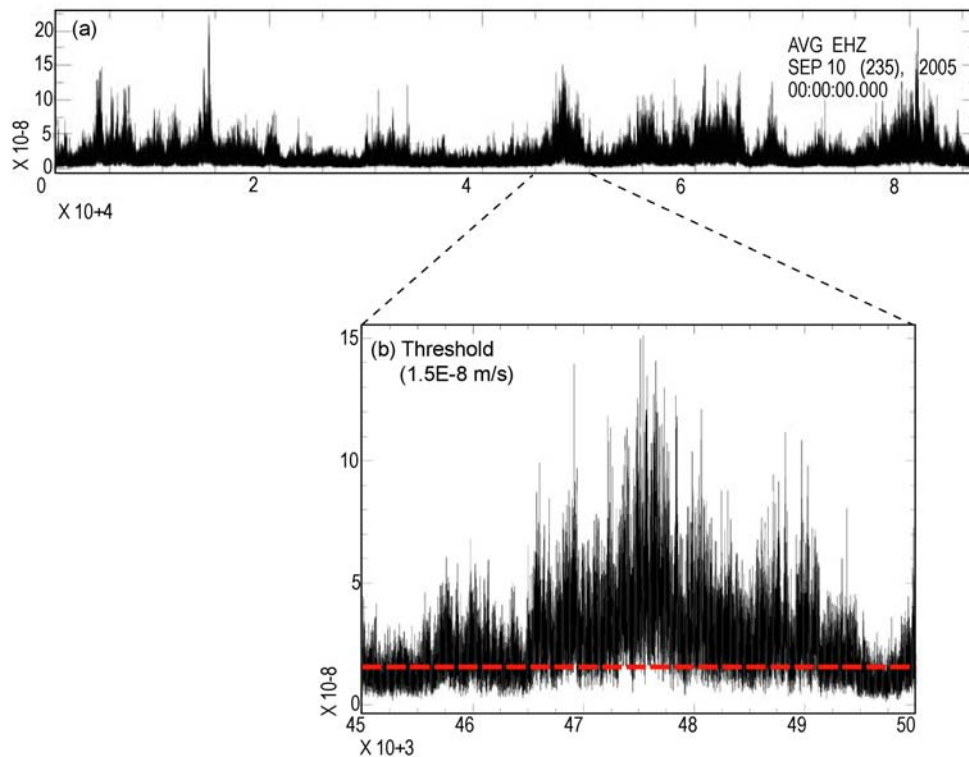

Figure 5. Example of the data average for day 253 of 2005. (a) Average of all the envelope functions of the stations that survived the data processing and cutting on day 253 of the year 2005. (b) Area of that day showing in detail how threshold value (red dashed line) is picked using a high tremor day.

Using this method, tremor was counted for all the collected data, which goes from June of 2005 to February of 2007. The threshold value varied a lot during this period, being lower during times of high tremor and GPS detectable events; and higher during times of no detectable events. Even though there are no tremor bursts correlating across stations during the times of no detectable events, the noise signal is predominant in these times and as different stations are averaged the noise amplitudes get enlarged. As mentioned before, this time period contains two of the latest SSE which are the September 2005 event and the January 2007 event (Figure 6).

Taking into account all ~19 months of data, 627.5 hours of tremor were counted of which 284.95 hours come from the September 2005 event and 238.38 hours belong to the January 2007 event. It is very clear on Figure 6 where the two GPS-detectable events are. The results show that around 80% of the total energy released during the ~19 months is released during the big events, but ~20% of the energy was released during other times, when there are no detectable GPS events.

<div align="center">Moment Magnitude—Tremor Time Relationship</div>

It is now known how many hours of tremor occurred during both the 2005 and 2007 events which correlate well with results from different research groups (McCausland *et al.*, 2005) which have also counted the hours of tremor for additional previous events starting in 2003 (McCausland *et al.*, 2005). These results are shown in Table 2.

Each of these events has already been assigned a slip distribution calculated from GPS (Szeliga *et al.*, 2007), which where used to calculate the inferred moment magnitude
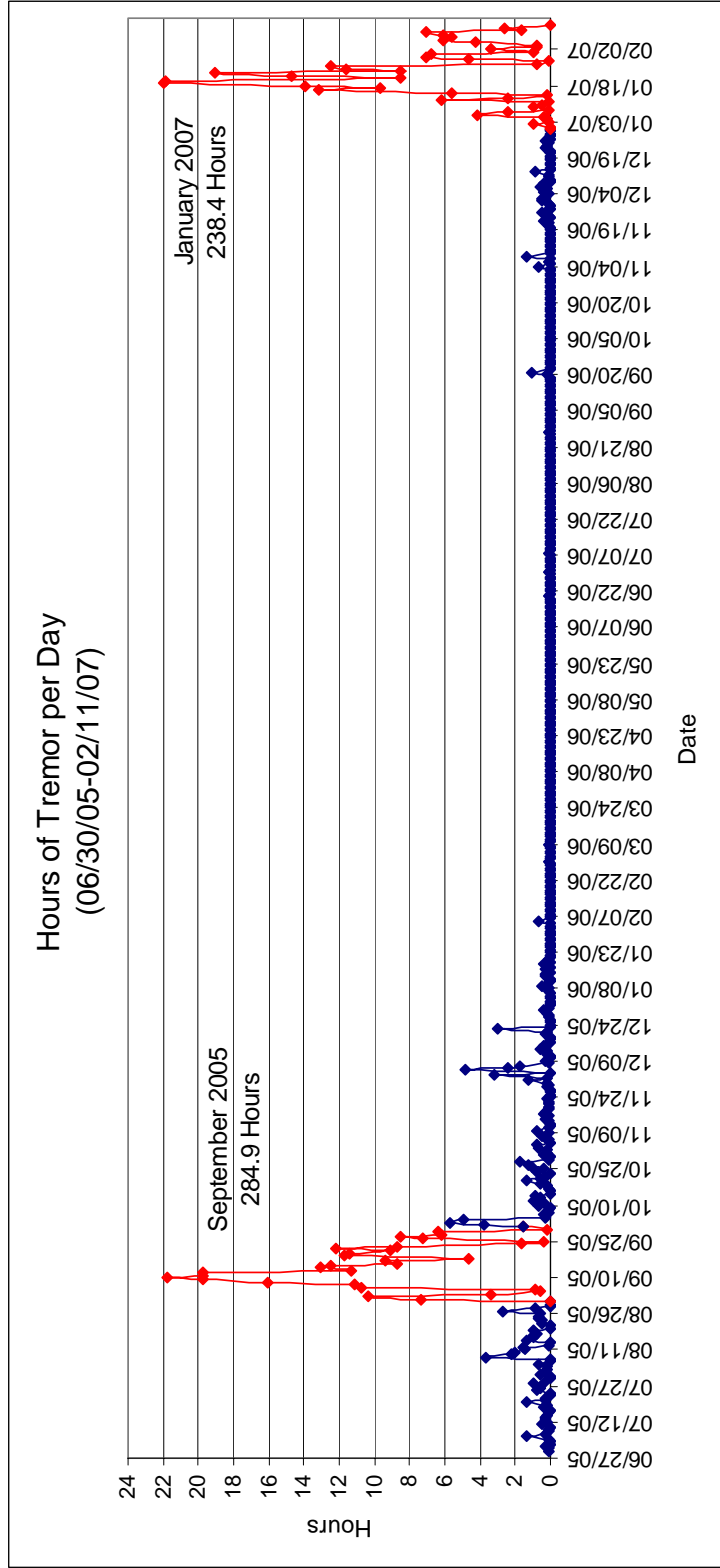
Figure 6. Counted hours of tremor. These were calculated using the averages of the envelope functions for each day of the year from June 30, 2005 to February 11, 2007. The red lines represent the two big events encompassed in the requested data which are the September 2005 event with 284.9 hours of tremor and the January 2007 event with 238 hours of tremor, and the blue lines represent the rest of the time. It is apparent that during 2006 there was little tremor activity.

Table 2
Hours of Tremor per GPS Event

Event	Hours of tremor
2007-January	238.4
2005-September	284.9
2005-April	111.9*
2004-July	251.5*
2004-May	164.6*
2004-January	66.5*
2003-February	111.8*

* Calculated by McCausland *et al.* (2005).

for each of the events. With this, the hours of tremor can be related to the inferred

moment by using the definition of moment magnitude,

$$M_W = \frac{2}{3} \log M_0 - 10.7.$$

By rearranging this equation we get

$$M_0 = 10^{\frac{3}{2}(M_W + 10.7)},$$

where M_0 is the inferred moment and is measured in dyne-cm. The results obtained from

this are shown in the graph in Figure 7.

The February 2003 event does not correlate with the other events and was not

included in the calculation of the best fit. The slip distributions calculated for this event

show it to be among the largest observed in Cascadia (Melbourne *et al.*, 2005; Szeliga *et*

al., 2007), whereas the Canadian analysis does not extend south of the border. The results

do not agree, hence it needs further investigation. Also, the seismic coverage on the

southern part of the Puget Sound (where the event concluded) was, at the time of the
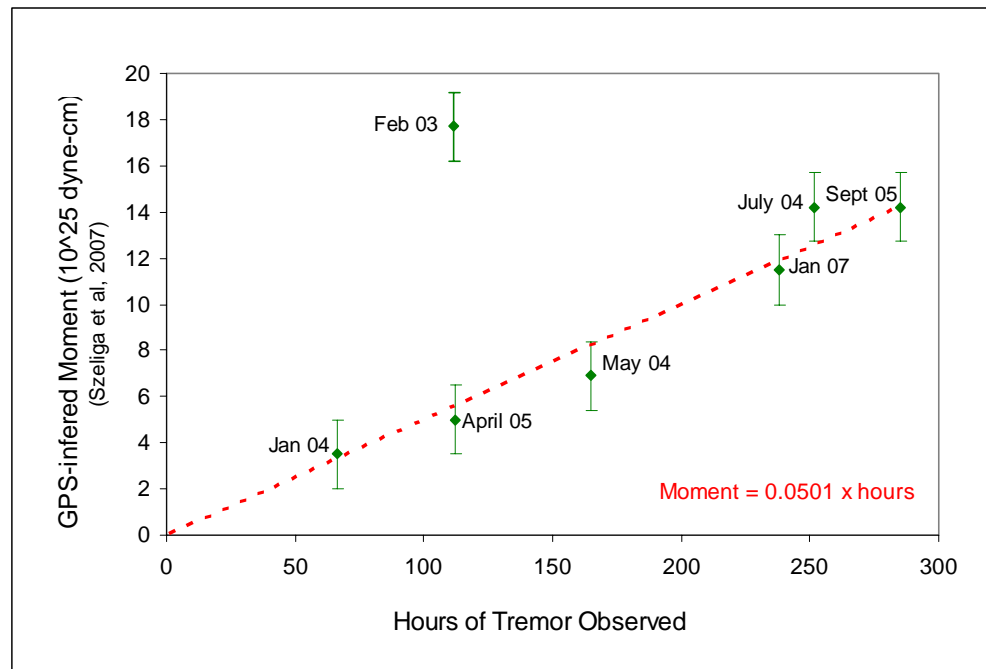
Figure 7. Graph of hours of tremor against GPS-inferred moment. It shows the values obtained by McCausland *et al.* (2005) and values calculated for this thesis against the inferred moment computed from GPS by Szeliga *et al.* (2007). The green lines represent the uncertainty (± 1.5 dyne-cm) and the red dashed line represents the best fit to the data points pinned to the origin.

event, not ideal and it is possible that the hours of tremor counted are lower than they should be. For this reason, there won't be any additional use of this event in the remaining sections of this thesis.

Given this exclusion, the relationship obtained from the inferred moments and the hours of tremor of the past events is

$$M_0 = 0.0501 \times 10^{25} \text{ dyne-cm} \times \text{hours of tremor} ,$$

with an uncertainty of ± 1.5 dyne-cm for the inferred moment.

It is been assumed here that zero hours of tremor mean that there is no released energy which is equivalent to zero moment. To apply this assumption, the best fit of the

events was pinned to the origin; therefore the data also suggests that the best fit line

includes the origin.

Discussion

The relationship obtained is linear; it shows that the moment is directly

proportional to the duration of tremor. Any event shorter than approximately 60 hours of

tremor cannot be seen by GPS. Because of its resolution, the smallest moment magnitude

that can be calculated is 6.3. But with this model it is possible to obtain magnitude values

for any tremor burst, even the smallest ones that can't be seen with GPS. As an example,

Table 3 shows moment magnitude values calculated using the moment magnitude—

tremor time model for different tremor times, ranging from 250 hours of tremor to just a

few minutes of tremor.

Table 3
Values for Different Tremor Times Calculated Using
the Magnitude-Time Model

Hours	Moment Magnitude (M_w)	Minutes	Moment Magnitude (M_w)
250	6.67	55	5.04
200	6.60	50	5.02
150	6.52	40	4.95
100	6.40	30	4.87
50	6.20	20	4.75
10	5.74	10	4.55
5	5.54	5	4.35
4	5.47	4	4.29
3	5.39	3	4.20
2	5.27	2	4.09
1	5.07	1	4.88

So, a magnitude can be assigned for each of the tremor bursts detected during a specific event. The January 2007 event is composed of ~5 bigger tremor bursts, so the model was used to determine the magnitude equivalence of each of these separate bursts (Figure 8).
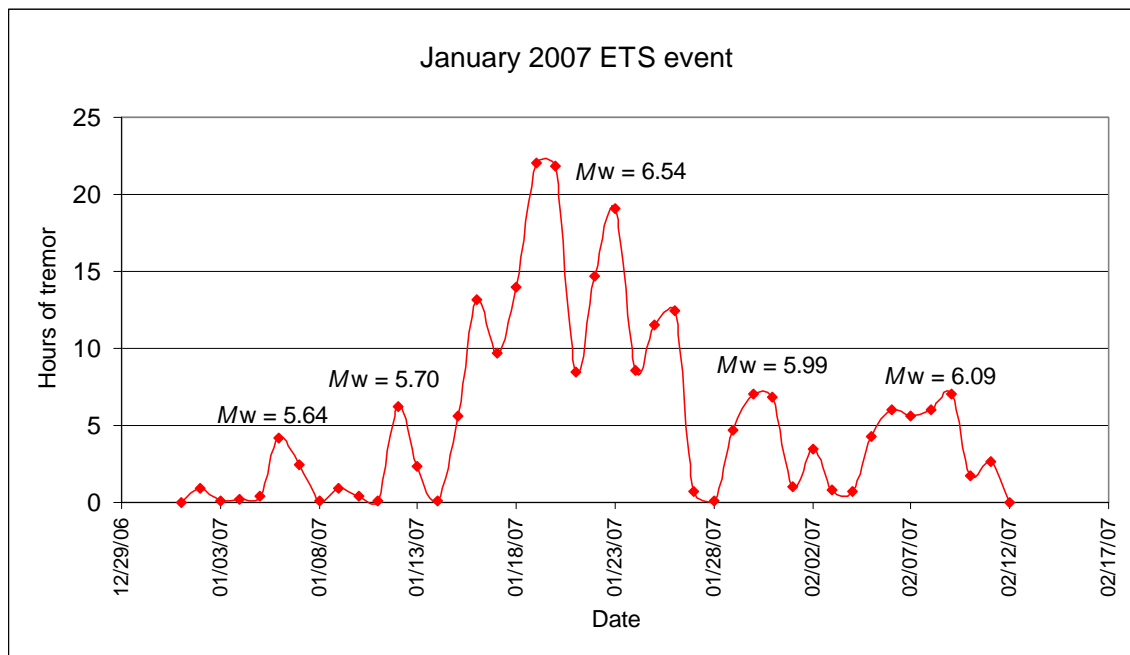
Figure 8. Enlargement of the January 2007 event. Each of the peaks is considered as a separate tremor burst. The amounts of hours for each of those peaks is represented above in moment magnitude calculated using the model.

Using this model, a histogram of all the tremor bursts that occurred during both the September 2005 and January 2007 events was created to see what type of frequency—magnitude relationship these ETS events follow (Figure 9).

From Figure 9 it can be inferred that tremor data for both events follow a log-linear frequency—magnitude relationship, which is similar to that of regular earthquakes. The b-values of 2.4 and 2.8 are higher than typical ranges known for regular tectonic
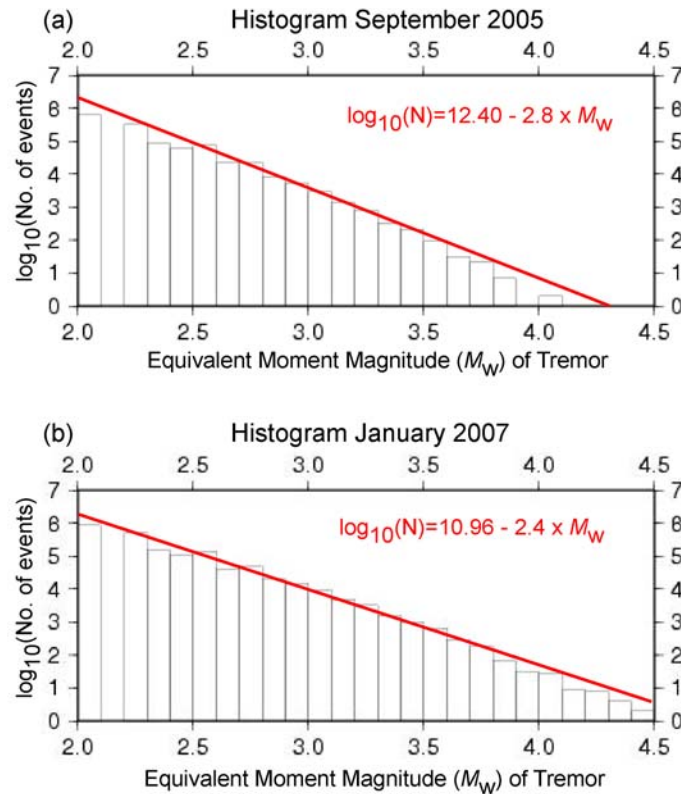
Figure 9. Histograms of the September 2005 and the January 2007 events. (a)Distribution of the duration of all the tremor bursts for the September 2005 event. (b) Distribution of the duration of all the tremor bursts for the January 2007 event. The red line in both graphs represents the least squares approximation of the results.

environments, which range from 0.8 to 1.2, indicating that this region favors smaller events. This is consistent with recent studies from Shelly *et al.* (2007) and Ide *et al.* (2007) suggesting that the subduction zone slow slip events are comprised of many small shear-slip events occurring in rapid succession.

From the present model, it is known that as the duration of tremor increases, the magnitude also increases, but the amplitude of the tremor does not vary much. This is not so for regular earthquakes; where velocity amplitudes increase as magnitudes increase. This is shown in Figure 10 using data from both of the GPS-detectable events.
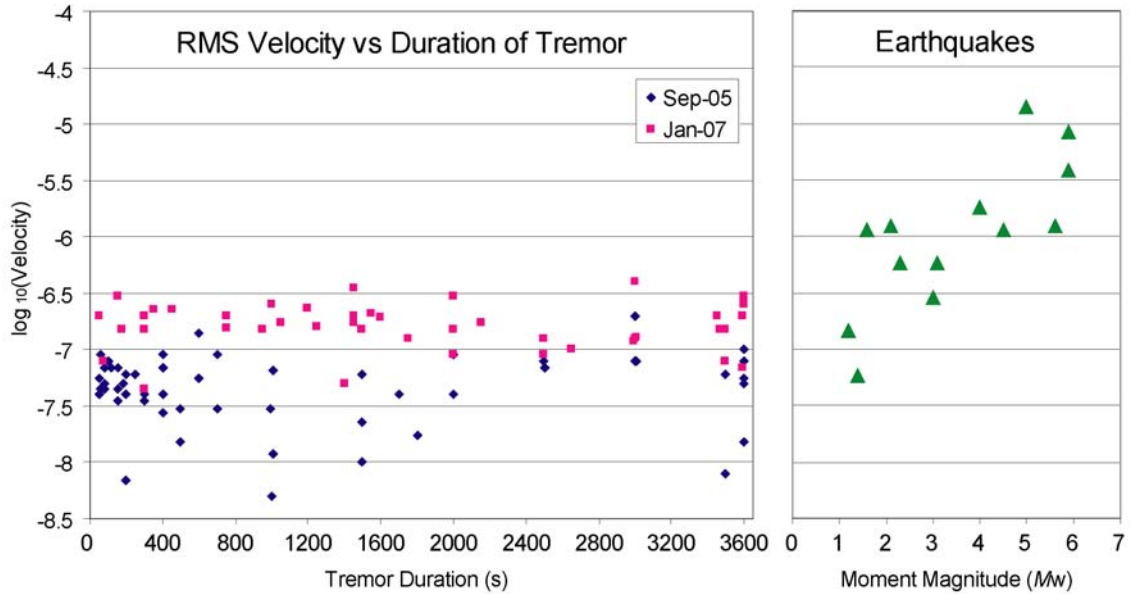
Figure 10. Comparison of amplitudes. The amplitudes of different length tremor bursts are compared to the amplitudes of earthquakes of different magnitudes. The blue diamonds represent tremor bursts that occurred during the September 2005 event and the pink squares represent tremor burst from the January 2007 event. The green triangles represent earthquakes of different magnitude that happened around the area.

One reason to believe that this model is correct is that it is consistent with the scaling law presented by Ide *et al.* (2007) which was a result of taking into account all the different manifestations of this phenomenon: low-frequency tremor, LFE, VLF earthquakes, and SSE. This scaling law is as follows:

$$M_0 \approx T \times 10^{12-13} \ \text{N-m},$$ (1)

where *T* is in seconds.

Now, the present model was solved for hours of tremor, so it is necessary to calculate the equivalent model with *T* in seconds instead of hours. This is

$$M_0 = \left(1 \times 10^{-5}\right) T \times 10^{25} \ \text{dyne-cm}.$$

The units here are dyne-cm, so it is necessary to convert the result to N-m:

$$M_0 = \left(1 \times 10^{-5}\right)\left(T \times 10^{25}\,\text{dyne-cm}\right)\left(\frac{1 \times 10^{-5}\,\text{N}}{1\ \text{dyne}}\right)\left(\frac{1\ \text{m}}{100\ \text{cm}}\right).$$

With these multiplications we get

$$M_0 = T \times 10^{13}\ \text{N-m},$$

with T in seconds which is equivalent to (1). This is also shown in Figure 11, with a plot of event duration against moment/moment-magnitude for all the different manifestations of this phenomenon, including the results obtained from the present model.

One last thing to mention here is that due to the filtering processes applied to the data (band-passing methods), it is not possible to see the long-period events and VLF earthquakes if they were present in the data; but it still makes sense to use this relationship because the VLF earthquakes are probably minor contributors during the big GPS events. Nevertheless, it is possible that VLF earthquakes bias the tremor scale, in which case the true scale should be displaced upwards on Figure 7 and it wouldn't be pinned to the origin.
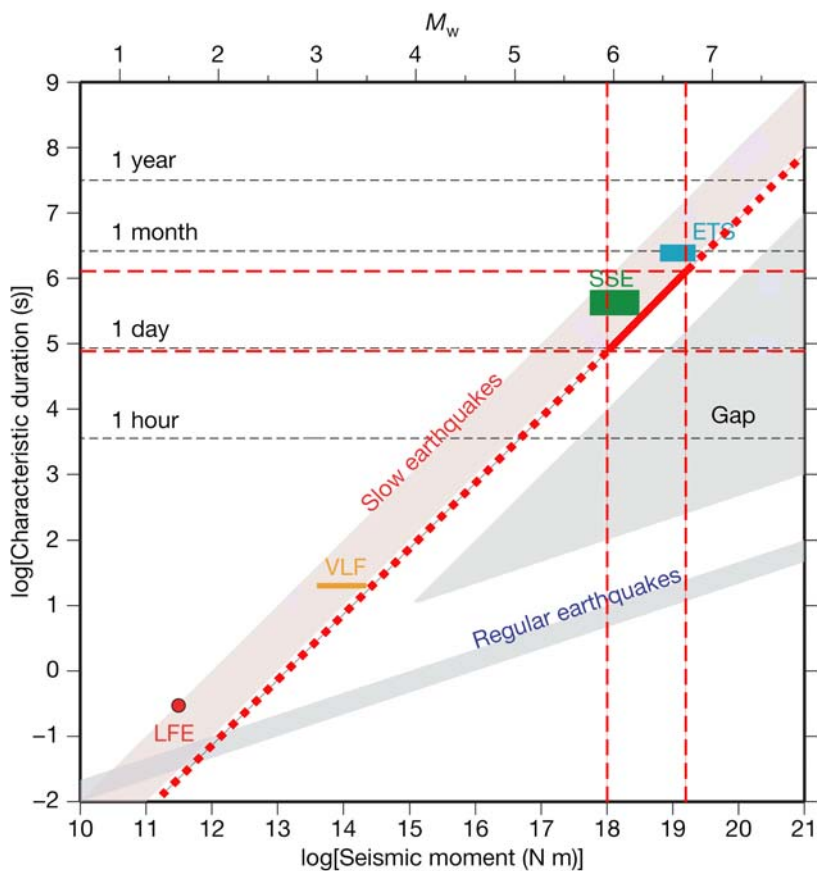
Figure 11. Comparison between Ide *et al.* (2007) scaling law and the current model. The LFE (red dot), VLF (orange bar), and SSE (in green) originate in the Nankai trough; and the ETS (in light bleu) originate in the Cascadia subduction zone. All these types of events follow the Ide *et al.* (2007) scaling law. The red dashed lines represents where the current model plots in the same scale, and the thick red line is the result shown in Figure 7. Both of these are very different from the regular earthquakes scale shown with a thick blue line. Modified from Ide *et al.* (2007).

CHAPTER IV

TREMOR LOCATIONS

After quantifying the tremor duration during a slow slip event, some of the tremor bursts were located. Since it is not possible to pick onset times for tremor, tremor was located using another approach. The location process was done only for the January 2007 event.

One-Dimensional S-Wave Velocity Model

To accomplish the location scheme, the plate interface was represented by a 60 × 24 grid called 60×24_Cascadia.latlondepth (Figure 12). Each line of this file contains one of the 1440 grid points and its respective surface coordinates. Using this type of grid means assuming that the tremor bursts originated on the plate interface, so only the surface view of the locations is going to be presented in this section. With this, it was necessary to know the travel times of the S-waves from each of the grid points to each of the stations of the requested data. The TauP Toolkit (Crotwell *et al.*, 1999) was used for this purpose.

The TauP Toolkit:

Flexible Seismic Travel-time and Ray-path Utilities

TauP is a software package designed to allow quick calculations of the position and timing of most seismic phases (e.g., P, S, ScS, Pp, etc). The function used from the
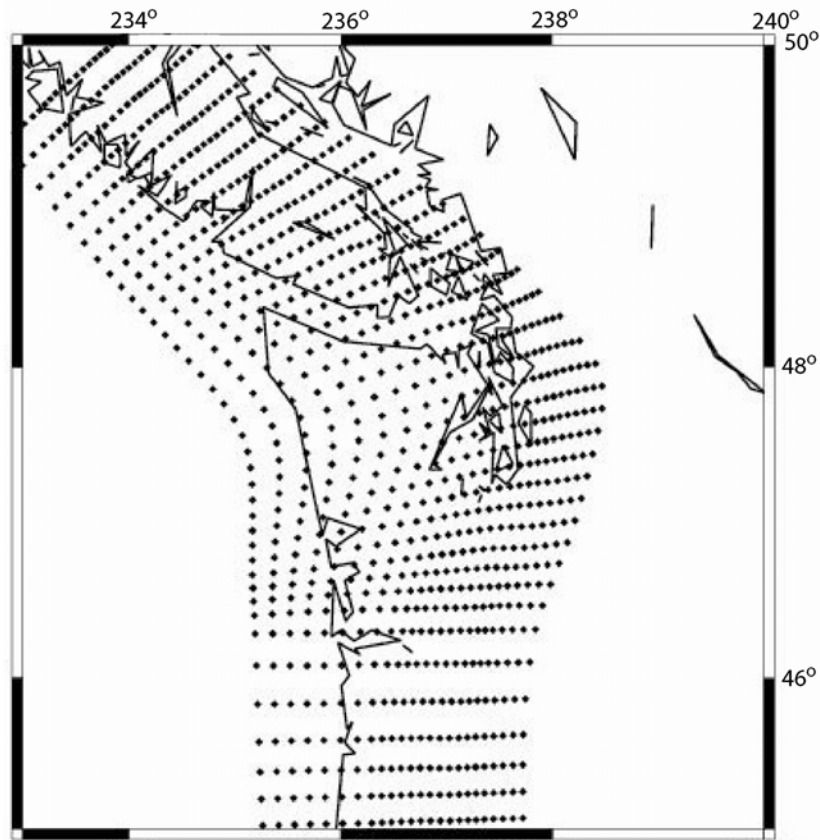
Figure 12. Surface projection of the 60 × 24 grid. This only shows the northern part of the grid which represents the plate interface of the Cascadia subduction zone.

toolkit was TauP_Time, which generates a travel time for a specified phase through a given earth model.

The s and S phase travel times from each of the grid points to each of the stations was calculated using this function with an S-wave velocity model called the Cascadia_P3 model. The complete velocity model is shown in the Appendix. All this information was stored in a file with 1440 lines; where each line represents one of the grid points and contains all the stations with its respective travel time from that same grid point. This file was named traveltimes_out.txt for further use and looks like the example presented below (Figure 13).

```
A04A 215.90 B001 198.47 B004 201.37 B005 201.37 B006 198.31…
A04A 210.74 B001 193.27 B004 196.01 B005 196.01 B006 193.06…
A04A 205.57 B001 188.05 B004 190.64 B005 190.64 B006 187.78…
A04A 200.37 B001 182.81 B004 185.24 B005 185.24 B006 182.49…
….
```

Figure 13. Example of traveltimes_out.txt. This file contains the travel times from each grid point to each station and it has the same number of lines as the grid file that was used to create it.

Differential Travel Times

Once the travel times to all the stations from the different depths were known, it was necessary to calculate the differential travel times between stations for each grid point. So, for each line of traveltimes_out.txt, the differential travel time was calculated for each pair of stations and saved in another file, with the same format as the last in which each line represents one grid point. This new file contains all the pairs of stations followed by the predicted differential travel time between those two stations for each of the grid points. The format of this file is the second station arrival time with respect to the first station, so + 10 seconds implies that the wave reached the second station 10 seconds after the first station. It was named diff_traveltimes_out.txt and is similar to the one shown in Figure 14,

```
B001 B006 -0.21 B001 D04A -21.93 B001 GMW -11.27 B001 BLN -0.54…
B001 B006 -0.27 B001 D04A -21.84 B001 GMW -11.20 B001 BLN -0.51…
B001 B006 -0.32 B001 D04A -21.74 B001 GMW -11.12 B001 BLN -0.49…
B001 B006 -0.37 B001 D04A -21.65 B001 GMW -11.04 B001 BLN -0.46…
….
```

Figure 14. Example of diff_traveltimes_out.txt. This file contains the synthetic differential travel times between stations. The first station represents the main station, so the number represents the time that it took the signal to get to the second station before (-) or after (+) the main station. This file has the same number of lines as the grid file used to create it.

Correlation of Stations

The correlation process was applied to small tremor bursts that could be seen in a group of stations. The bursts were chosen in the following manner: if it was a small tremor burst of approximately 20–100 s, and it was detected by at least four stations, it was selected and cut out of the data set to be correlated between stations. Each station file was correlated with all the other station files using a C++ program called correlate.cxx, which outputs a sac file that was named corr_file1_file2.sac. By using SAC, the observed differential travel times between the pairs of stations where picked and saved. After acquiring all the differential times for all the pairs of stations for that specific tremor burst, they where saved in a one line file similar to the following:

2007011545000 CPW MEW 1.019 0.153 GMW GNW 0.628 0.105 GMW MEW
2.398 0.133 GNW MEW 0.207 0.203 HDW B006 4.229 0.426 …

Figure 15. Example of the correlation file. This is used to locate tremor bursts; it shows the date and time of the tremor burst, the pairs of stations that were correlated, the hand picked differential travel time between those two stations, and the weight of the correlation.

First, this file shows the year, month, day, and second when the burst occurred; it then displays each pair of correlated stations, the respective hand picked differential travel time between those two stations, and the weight of that correlation, which means how well the two stations correlate. Each correlation file has amplitudes between zero and one, where zero means the two files do not correlate at all, and one means a perfect correlation. The weight value was calculated in the following manner:

$$weight = 1 - \text{amplitude value}.$$

Knowing the weight value, the tremor location can now be done. The method used to locate the tremor was to minimize the L2 norm of the measured differential travel times minus the predicted differential travel times. As an example, let's say the correlation was done using 4 different stations with names A, B, C, and D. The L2 norm for this particular correlation would be as follows:

$$L2_{norm} = \frac{\sqrt{\left(\frac{\tau_{AB}-\tau_{AB'}}{weight_{AB}}\right)^2 + \left(\frac{\tau_{AC}-\tau_{AC'}}{weight_{AC}}\right)^2 + \left(\frac{\tau_{AD}-\tau_{AD'}}{weight_{AD}}\right)^2 + \left(\frac{\tau_{BC}-\tau_{BC'}}{weight_{BC}}\right)^2 + \left(\frac{\tau_{BD}-\tau_{BD'}}{weight_{BD}}\right)^2 + \left(\frac{\tau_{CD}-\tau_{CD'}}{weight_{CD}}\right)^2}}{No.of\ pairs}\ ,$$

where τ_{AB} is the measured differential travel time obtained from the correlation, $\tau_{AB'}$ is the predicted differential travel time obtained from diff_traveltimes_out.txt, and $weight_{AB}$ is the weight value obtained from the correlation of station A with station B. So, for one correlation file, the L2 norm was calculated using values of each of the lines of diff_traveltimes_out.txt, one at a time, until the lowest value of the L2 norm was found. The number of the line from which the L2 norm value was the lowest (Note: diff_traveltimes_out.txt has 1440 lines) represents the location of the tremor bursts. The coordinates of the surface projection of the location were now obtained from the same line number in the grid file, which, as mentioned before also has 1440 lines.

Using this method, 47 tremor bursts from the January 2007 event were processed and located (Figure 16).

The results obtained show a northwestward motion of source locations with time (represented by the color change from blue to red) across the southern Puget Sound during the January 2007 event.
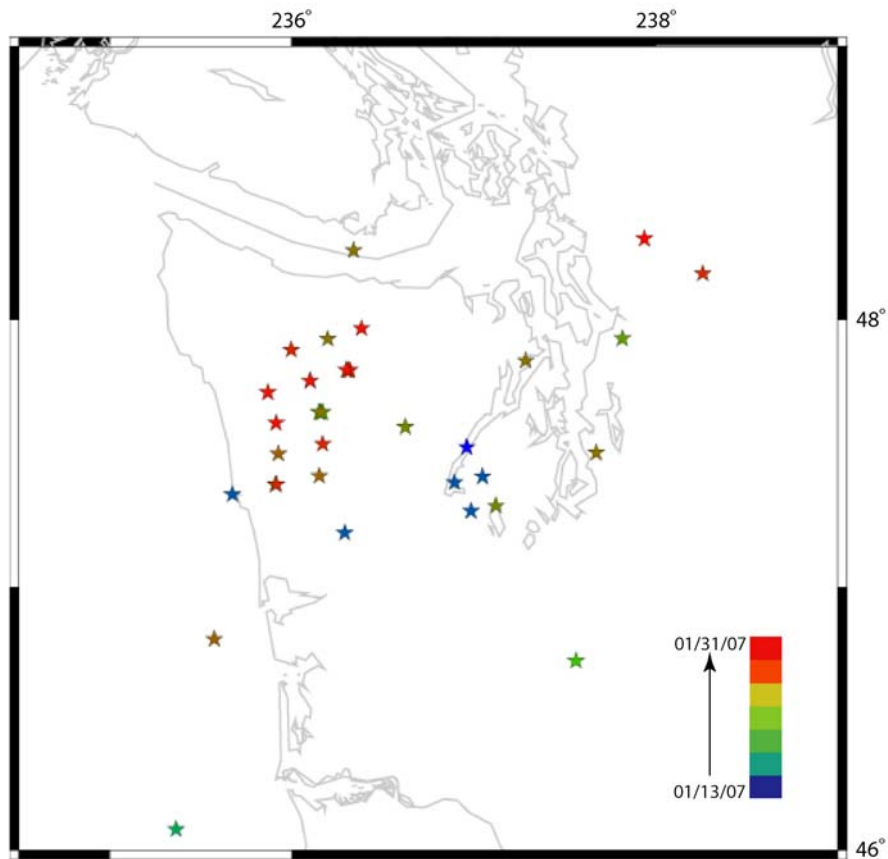
Figure 16. Surface projection of the locations of tremor bursts from the January 2007 event using a 1D grid. There are 47 locations plotted here that were done using a 60×24 grid representing the plate interface. The color of the stars changes as the day of the month advances going from blue to green to red.

Three Dimensional (3D) Grid

Since the grid used before does not take into account the depths of the locations of the tremor bursts, instead placing them automatically on the plate interface, the analysis was repeated with another type of grid. This new grid formed a cube of $60 \times 60 \times 21$ squares covering the same area but going as deep as 70 km everywhere. The same process for the correlation mentioned before was followed using this new 3D grid and the original 47 events were located again (Figure 17).
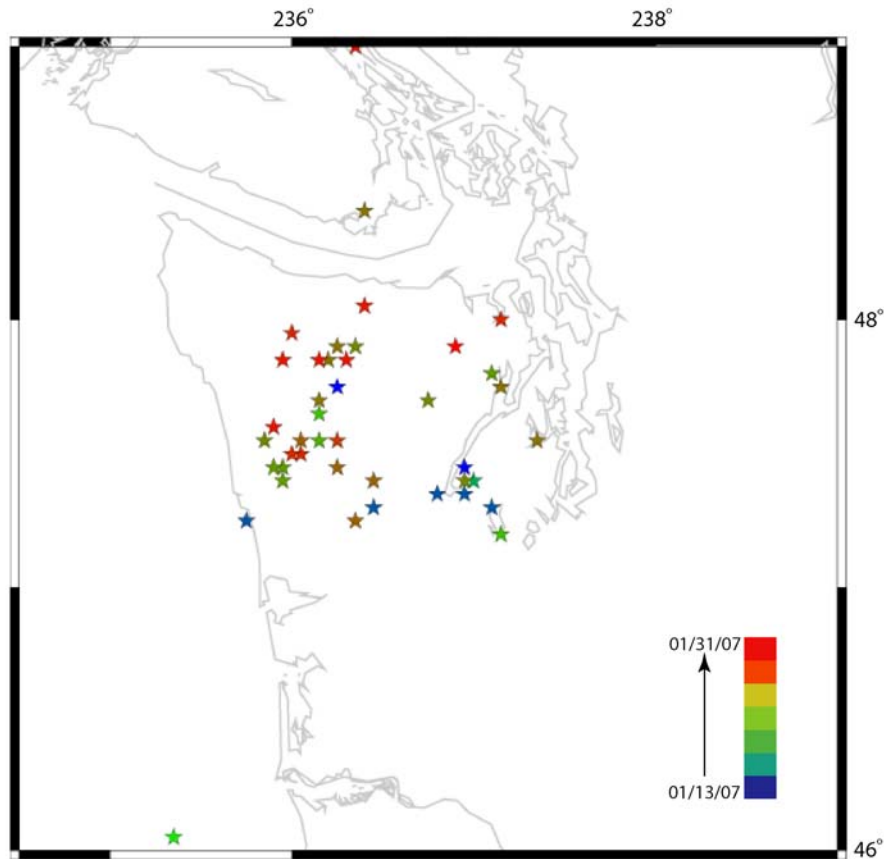
Figure 17. Surface projection of the locations of tremor bursts from the January 2007 event using a cube grid. There are 47 locations plotted here that were done using a 60 × 60 × 21 cube grid. The star color changes as the day of the month advances, going from blue to green to red.

The locations of the 47 tremor events on to the 3D cube grid (Figure 17) seem

significantly tighter compared to the locations on the 60 × 24 grid (Figure 16). There are

no events located east of the Puget Sound and there are fewer events to the south. It can

be observed from Figure 17 that the cube grid is a much finer grid. This clearly reduced

the overlapping of a few events making it easier to observe all the tremor bursts. A

northwestward motion over time of the tremor locations from the January 2007 event can

also be observed on this grid, starting with the blue stars on the southern Puget Sound,

finishing with the red stars northwest of the Puget Sound.

Discussion

The 60×24 grid clearly was not fine enough because it was possible to observe

(Figure 16) the grid points on the surface view of the locations of the tremor bursts. This

was one of the reasons that the 3D cube grid was made finer to reduce the overlapping of

events (Figure 17). As we compare these locations to the slip distribution of this

particular event calculated from the GPS inversions (T. Melbourne, unpublished results,

2007) it is evident that the majority of the locations are west of where the motion was

shown to be from these inversions (Figure 18).

Most of these locations are also west of the results for tremor locations presented

on the PNSN Database (2007) which show only a northern movement as the day of the

month increases, as it is shown from the slip distributions (Figure 18). One of the reasons

that the results obtained are west of the slip is that the correlation process is highly

influenced by the group of stations that were correlated for a particular burst, where it

seems to locate the tremor closer to that specific group of stations. This might have

happened to a few of the locations. Nevertheless they are still located in the vicinity of

the slip distribution, in areas that have shown to be active with tremor during past GPS

events (McCausland *et al.*, 2005).

It is necessary to talk about the depths of these locations. All the tremor bursts

located were found to be between the 20- to 40- km depth contours of the plate
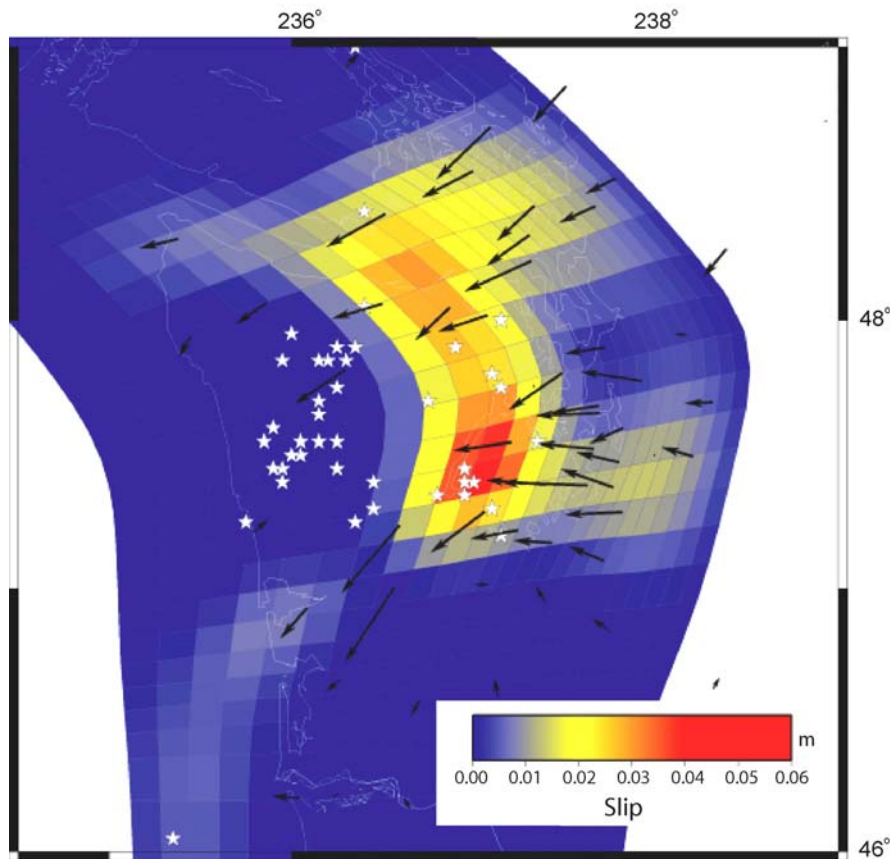
Figure 18. GPS-inferred slip distribution from the January 2007 event (T. Melbourne, unpublished results, 2007). The white stars represent the locations of the 47 tremor bursts from the 2007 event. The black arrows are the measured GPS offsets.

interface as shown in Figure 19, but the calculated depths where not constrained to the plate interface. Instead, they where located to the bottom layer of the grid, which means that this method was not able to solve for the depths, just the surface projections.

However, previous studies have shown that the surface projections of the locations of tremor bursts for past events has also been in approximately the same range of depth contours (Kao *et al.*, 2005; McCausland *et al.*, 2005; Kao *et al.*, 2006; Royle *et al.*, 2006), but their depths have been reported to be scattered on both the subducting slab and the overriding crust.
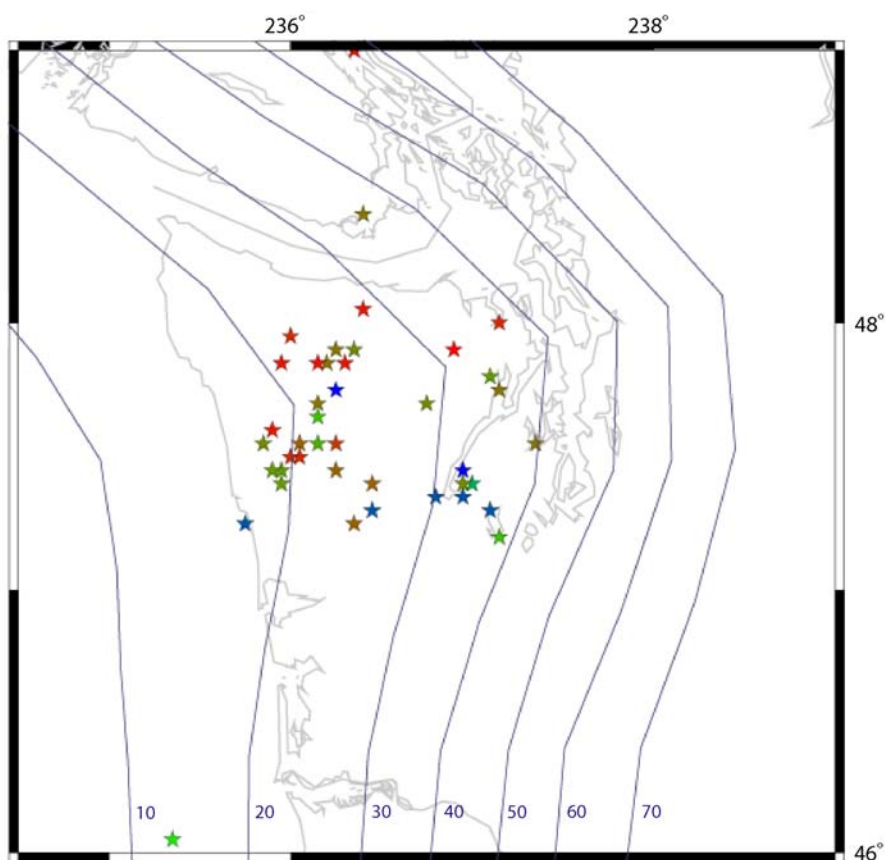
Figure 19. Surface projection of tremor locations for the January 2007 event with the depth contours of the plate interface. The numbers represent the depth of the Cascadia subduction zone on each specific contour (blue lines).

Slip distributions determined from GPS SSE signals along with the locations of tremor may delineate where the transition/locked zone is, and if so they seem to indicate that it is somewhere around the 30 km (Szeliga *et al.*, 2007) depth contour of the plate interface (Figure 18). This argument implies that the potential seismic hazard from a megathrust rupture is far greater than models that place the locked zone off shore (Savage and Lisowski, 1991; Hyndman and Wang, 1993; Dragert and Hyndman, 1995; Hyndman and Wang, 1995). It suggests that the locked zone lies near the western edge of the

Seattle metropolitan basin, under which a large earthquake would certainly be

catastrophic.

CHAPTER V

CONCLUSIONS

In conclusion, it was shown that the 1 to 5 Hz band tremor can be used to study the shorter duration slip events that can not be observed with GPS. Because of this, tremor helps quantify moment release over time in great detail. It shows that tremor duration is directly proportional to the GPS inferred moment magnitude, assuming we ignore the low frequency events, such as LFE and VLF earthquakes, if in fact they exist in Cascadia. The present model agrees extremely well with Ide et al. (2007) scaling law for the slow earthquakes, and with it, it was found that tremor follows a strikingly log–linear frequency—moment relationship characteristic of earthquakes. The b-values are greater than typical ranges (> 2.4) known for regular tectonic environments (0.8–1.2), indicating that the region favors smaller events. This is consistent with new studies suggesting that subduction zone slow slip events are comprised of many very small events occurring in rapid succession.

For the January 2007 event, the locations of the tremor bursts suggest a northwestward movement, and the slip distributions show a northward movement. This discrepancy may be due to the fact that the locations were heavily influenced by the group of stations used during the correlation process. Nevertheless, they are still in the vicinity of the GPS slip inversions and locate to the range of 20- to 40- km depth contours, agreeing with results for past GPS-detectable events.

Finally, as suggested from the slip and tremor locations together, there is a possibility that the transition/locked zone is closer to the 40- km depth contour of the

plate interface, which means closer to a major city and greatly increases the seismic hazard of the subduction zone. This shows the importance of this study and the potential for tremor to be used in the mapping of seismic hazards. More work should be done in order to reduce the uncertainties involved in the location process so it can be applied not only in the Cascadia subduction zone, but also in other large subduction zones where similar processes are occurring.

REFERENCES

Atwater, B. F. (1987). Evidence for great Holocene earthquakes along the outer coast of Washington State, *Science* **236**, 942–944.

Atwater, B. F., and E. Hemphill-Halley (1997). Recurence intervals for great earthquakes of the past 3500 years at northwestern Willapa Bay, Washington, *US Geol. Surv. Prof. Pap.* **1576**, 1–108.

Atwater, B. F., M. R. Satoko, S. Kenji, T. Yoshinobu, K. Ueda, and D. K. Yamaguchi (2005). The orphan tsunami of 1700, Japanese clues to a parent earthquake in North America, *U.S. Geol. Surv. Profess. Pap. 1707*, 144 pp.

Crotwell, H. P., T. J. Owens, and J. Ritsema (1999). The TauP Toolkit: Flexible Seismic Travel-time and Ray-path Utilities, *Seism. Res. Lett.* **70**, 154–160.

Dragert, H., and R. D. Hyndman (1995). Continuous GPS monitoring of elastic strain in the norther Cascadia subduction zone, *Geophys. Res. Lett.* **22**, NO. 7, 755–758.

Dragert, H., K. Wang, and T. S. James (2001). A silent slip event on the deeper Cascadia subduction interface, *Science* **292**, 1525.

Hirose, H., and K. Obara (2005). Repeating short- and long-term slow slip events with deep tremor activity around the Bungo channel region, southwest Japan, *Earth Planets Space* **57**, 961–972.

Hyndman R. D., and K. Wang (1993). Thermal constraints on the zone of major thrust earthquake failure: The Cascadia subduction zone, *J. Geophys. Res.* **98**, no. B2, 2039–2060.

Hyndman R. D., and K. Wang (1995). The rupture zone of Cascadia great earthquakes from current deformation and the thermal regime, *J. Geophys. Res.* **100**, no. B11, 22,133–22,154.

Ide, S., G. Beroza, D. Shelly, and T. Uchide (2007). A scaling law for slow earthquakes, *Nature* **447**, 76–79.

Ide, S., D. Shelly, and G. Beroza (2007). Mechanism of deep low frequency earthquakes: Further evidence that deep non-volcanic tremor is generated by shear slip on the plate interface, *Geophys. Res. Lett.* **34**, L03308, doi:10.1029/2006GL028890.

Ito, Y., K. Obara, K. Shiomi, S. Sekine, and H. Hirose (2007), Slow earthquakes coincident with episodic tremors and slow slip events, *Science* **315**, 503–506.

Kao, H., S. Shan, H. Dragert, G. Rogers, J. F. Cassidy, and K. Ramachandran (2005). A wide depth distribution of seismic tremors along the northern Cascadia margin, *Nature* **436**, 841–844.

Kao, H., S. Shan, H. Dragert, G. Rogers, J. F. Cassidy, K. Wang, T. S. James, and K. Ramachandran (2006). Spatial-temporal patterns of seismic tremors in northern Cascadia, *J. Geophys. Res.* **111**, B03309, doi:10.1029/2005JB003727.

Linde, A. T., K. Suyehiro, S. Miura, I. S. Sacks, and A. Takagi (1988). Episodic aseismic earthquake precursors, *Nature* **334**, 513–515.

McCausland, W., S. Malone, and D. Johnson (2005), Temporal and spatial occurrence of deep non-volcanic tremor: From Washington to northern California, *Geophys. Res. Lett.* **32**, L24311, doi:10.1029/2005GL024349.

Melbourne, T. I., F. H. Webb, J. M. Stock, and C. Reigber (2002). Rapid postseismic transients in subduction zones from continuous GPS, *J. Geophys. Res.* **107**, no. B10, 2241, doi:10.1029/2001JB000555.

Melbourne, T. I., W. M. Szeliga, M. M. Miller, and V. M. Santillan (2005). Extent and duration of the 2003 Cascadia slow earthquake, *Geophys. Res. Lett.* **32**, L04301, doi:10.1029/2004GL021790.

Miller, M., T. Melbourne, D. Johnson, and W. Sumner (2002). Periodic slow earthquakes from the Cascadia subduction zone, *Science* **295**, 2423.

Nadeau, R., and D. Dolec (2005). Nonvolcanic tremors deep beneath the San Andreas fault, *Science* **307**, 389.

Obara, K. (2002). Nonvolcanic deep tremor associated with subduction in southwest Japan, *Science* **296**, 1679–1681.

Ozawa, S., M. Murakami, M. Kaidzu, T. Tada, T. Sagiya, Y. Hatanaka, H. Yarai, and T. Nishimura (2002). Detection and Monitoring of Ongoing Aseismic Slip in the Tokai Region, Central Japan, *Science* **298**, 1009–1012.

Peterson, C., D. Christensen, and S. McNutt (2005). Episodic tremor in the Alaska/Aleutian Subduction Zone, *American Geophysical Union*, Fall Meeting 2005, abstract #G51B-0830.

PNSN Database. www.pnsn.org/WEBICORDER/DEEPTREM/tremorLocMap.gif (for tremor location map; accessed August 14, 2007).

Rogers, G., and H. Dragert (2003). Episodic tremor and slip on the Cascadia subduction zone: The chatter of silent slip, *Science* **300**, 1942–1943.

Royle. G. T., A. J. Clavert, and H. Kao (2006). Observations of non-volcanic tremor during northern Cascadia slow-slip event in February 2002, *Geophys. Res. Lett.* **33**, L18313,doi:10.1029/2006GL027316.

Satake, K., K. Shimazaki, Y. Tsuji, and K. Ueda (1996). Time and size of a giant earthquake in Cascadia inferred from Japanese tsunami records of January 1700, *Nature* **379**, 246–249.

Satake, K., K. Wang, and B. F. Atwater (2003). Fault slip and seismic moment of the 1700 Cascadia earthquake inferred from Japanese tsunami descriptions, *J. Geophys. Res.* **108**, doi:10.1029/2003JB002521.

Savage, J. C., and M. Lisowski (1991). Strain measurements and the Potential for a Great Subduction Earthquake Off the Coast of Washington, *Science* **252**, 101-103.

Shelly, D., G. Beroza, S. Ide, and S. Nakamula (2006). Low-frequency earthquakes in Shikoku, Japan, and their relationship to episodic tremor and slip, *Nature* **442**, 188–191.

Shelly, D., G. Beroza, and S. Ide (2007). Non-volcanic tremor and low-frequency earthquake swarms, *Nature* **446**, 305–307.

Szeliga, W., T. Melbourne, M. Miller, and M. Santillan (2004). Southern Cascadia episodic slow earthquakes, *Geophys. Res. Lett.* **31**, L16602, doi:10.1029/2004GL020824.

Szeliga, W., T. Melbourne, M. Santillan, and M. Miller (2007). 30+ slow slip events from the Cascadia Subduction Zone, 1997-2006, *J. Geophys. Res.* **In Review**.

Wang, K., R. Wells, S. Mazzotti, R. D. Hyndman, and T. Sagiya (2003). A revised dislocation model of interseismic deformation of the Cascadia subduction zone, *J. Geophys. Res.* **108**, no. B1, 2026,doi: 10.1029/2001JB001227.

APPENDIX

Cascadia_P3 P and S Phase Velocity model

Depth (km)	Vp (km/s)	Vs (km/s)	ρ (g/cm^3)
Surface			
0	5.40000	3.03000	2.60000
4	6.38000	3.58000	2.60000
9	6.59000	3.70000	2.60000
16	6.73000	3.78000	2.60000
20	6.86000	3.85000	2.70000
25	6.92000	3.88000	2.90000
41	6.95000	3.90000	2.90000
Mantle			
41	7.80000	4.38000	3.37000
60	8.08907	4.47715	3.37688
80	8.07688	4.46953	3.37471
115	8.05540	4.45643	3.37091